DNA Bending by bZIP Charge Variants: A Unified Study Using Electrophoretic Phasing and Fluorescence Resonance Energy Transfer†

Philip R. Hardwidge,‡ Jiong Wu,§ Sarah L. Williams,§ Kay M. Parkhurst,§ Lawrence J. Parkhurst,§ and L. James Maher, III*,‡

Department of Biochemistry and Molecular Biology, Mayo Foundation, Rochester, Minnesota 55905, and Department of Chemistry, University of Nebraska−Lincoln, Lincoln, Nebraska 68588-0304

Received March 15, 2002; Revised Manuscript Received April 22, 2002

ABSTRACT: The role of asymmetric charge neutralization as a primary determinant of protein-induced DNA helical bending remains controversial. Electrophoretic phasing experiments have been conducted previously for peptides derived from the yeast basic leucine zipper (bZIP) transcription factor GCN4 bound to AP-1 sites in duplex DNA. Mutations altering the electrostatic character of amino acids close to the DNA backbone result in phase-dependent gel mobility changes, interpreted as evidence of DNA bending. However, alternate interpretations are possible. The effect of electrostatic interactions on DNA conformation has now been investigated further, using purified peptides having indistinguishable AP-1 DNA affinity. Two independent techniques have been employed: electrophoretic phasing and fluorescence resonance energy transfer (FRET). The phasing results imply DNA bending by bZIP charge variants, consistent with earlier findings. FRET studies yield the mean 5′ end to 3′ end distance of AP-1 DNA when free or bound to neutral or charged bZIP peptides. These distances were reduced in the charged variant complexes relative to those in the free duplex and the wild-type complex. Bending of the DNA helical axis is shown by molecular modeling to be the simplest interpretation of these results. The electrophoretic phasing and FRET results thus offer two mutually supportive lines of evidence for induced bending of the DNA helical axis due to asymmetric changes in charge density caused by the electrostatic character of the amino acids residing near the DNA backbone.

DNA is commonly bent when bound by proteins (*1*). Protein-mediated DNA bending is believed to be important to many cellular processes, including the formation of nucleosomes and the assembly of nucleoprotein complexes required for transcription activation (*2*, *3*). Although most short DNA segments do not assume extreme conformations, protein binding releases sufficient free energy to drive the bending of DNA into compact, folded structures (*1*, *4*).

Two classes of DNA bending proteins have been recognized (*4*). Class 1 DNA bending proteins [e.g., TATA-binding protein (TBP)] contact DNA through intercalation of hydrophobic amino acids between base pairs in the minor groove, bending the DNA helix away from the protein (*5*, *6*). Class 2 DNA bending proteins (e.g., the histone octamer) contact DNA through electrostatic interactions between cationic amino acids and the DNA sugar−phosphate backbone (*2*). DNA deformation by class 2 DNA bending proteins often involves DNA bending toward the bound protein (*7*).

The role of electrostatic effects in DNA bending by class 2 proteins is an area of active investigation (*8*). DNA bending occurs when favorable interactions achieved between the DNA and protein are sufficient to overcome the costs of DNA deformation. To what extent do favorable electrostatic interactions contribute? To what extent do inherent interphosphate repulsions (stretching forces) allow DNA to resist deformation? To what extent does asymmetric charge neutralization of DNA phosphate charges induce spontaneous "collapse" of the DNA toward the protein? The present study is part of an ongoing series of experiments motivated by these questions (*4*).

Mirzabekov and Rich originally hypothesized that the approach of the cationic surface of a protein near the DNA backbone increases the screening of DNA phosphate charges relative to the screening otherwise due to condensed cations (*9*). This leads to an asymmetric decrease in phosphate−phosphate charge repulsions on the protein-bound face of the helix relative to the face away from the protein (*9*). The resulting unbalanced interphosphate repulsions are predicted to cause a collapse of the DNA backbone toward the protein (*10*). Important contributions to DNA bending are also undoubtedly made by both electrostatic attraction and the entropically favored displacement of counterions.

Induced bending of DNA has been investigated for various members of the family of basic leucine zipper (bZIP) proteins, including Fos-Jun, Jun-Jun, CREB, and GCN4. Different members of the bZIP family are thought to influence DNA architecture in different ways (*11*−*15*). In particular, three amino acids immediately N-terminal to the basic region of bZIP proteins reside very close to the DNA helix (*16*). Kerppola (*12*, *15*) and Schepartz (*14*) noted that

† Supported by the Mayo Foundation and NIH Grant GM54411 to L.J.M. and by NIH Grants GM59346 and CA76049 to L.J.P.

* To whom correspondence should be addressed.Tel: +1 507 284 9041. Fax: +1 507 284 2053. E-mail: maher@mayo.edu.

‡ Mayo Foundation.

§ University of Nebraska−Lincoln.

10.1021/bi020213w CCC: $22.00
Published on Web 05/24/2002

the presence of charged residues in these positions of other bZIP proteins correlates strongly with apparent DNA bending in the resulting protein−DNA complexes, as measured by electrophoretic phasing assays. Because GCN4 contains a neutral amino acid cluster (PAA) at this site, this model would predict the absence of GCN4-induced DNA bending. Consistent with this view is a GCN4−DNA cocrystal structure showing little deformation of the DNA duplex AP-1 target site (*16*). This result must, however, be considered in view of the fact that the crystallizing agents used in such studies have been shown to dramatically alter the extent of protein-induced DNA bending in some cases (*17*).

If interphosphate repulsion is a fundamental determinant of DNA shape, then substitution of cationic or anionic amino acids for the neutral PAA amino acids of GCN4 might be predicted to result in DNA bending. Electrophoretic phasing analyses supported this hypothesis: cationic amino acid substitutions resulted in an apparent DNA bend toward the protein-bound face, while anionic amino acid substitutions caused DNA bending away from the protein-bound face (*14*, *18*, *19*). A similar result was obtained in studies of bZIP−DNA complexes involving variants of Jun and Fos (*13*).

A number of limitations of the above experiments have been recognized. Gel methods (phasing analysis, circular permutation) used to study DNA bending are based on the premise that bent DNA molecules migrate more slowly through a gel matrix than unbent DNA molecules, corresponding to reduced end-to-end distance. These methods also assume that the shape of the DNA in a protein−DNA complex dominates the electrophoretic properties of the complex (*20*). Recent studies of bZIP−DNA complexes have raised the possibility that the extended shape of some leucine zipper domains of bound bZIP proteins may contribute substantially to the overall frictional coefficient of the complex detected by electrophoresis (*21*). Electrophoretic studies are also limited in that one cannot from first principles predict the relationship between molecular shape and mobility through a gel matrix. These concerns are somewhat diminished for the described GCN4 studies, since truncated peptides (representing only the DNA-binding domain of the protein) were used, an identical leucine zipper domain was present in all peptides, and only three amino acids were varied to create charge variants (*19*). Nonetheless, it is possible that different charge variants affect gel mobility due to some property other than DNA bending.

The most notable conflicting results have been those obtained for derivatives of the bZIP heterodimer Fos-Jun. Electrophoretic phasing studies indicate that some Fos-Jun derivatives induce a 15−30° bend in the DNA helix (*22*−*24*). However, cyclization kinetics, minicircle competition binding assays, and crystal structures all indicate that various related Fos-Jun derivatives do not bend DNA (*20*, *21*). Although some of this discrepancy may be due to inconsistency in the particular peptide constructs tested, electrophoretic phasing assays have been questioned in the analysis of DNA bending by bZIP proteins (*20*, *21*).

We have undertaken a unified study to further examine bZIP-induced DNA conformational changes using both electrophoretic phasing and fluorescence resonance energy transfer (FRET).[1] This work utilizes a new family of recombinant, purified bZIP charge variants derived from GCN4.

Time-resolved FRET measurements have been shown previously to yield precise bend angles for various DNA promoters bound to the TATA-binding protein (TBP), with mean interdye distances reliably determined to a precision of ~0.1 Å (*17*, *25*−*27*). Furthermore, excellent agreement has been demonstrated between FRET and crystallography in determining these induced bends for two consensus promoters, the major late and E4 sequences from the adenovirus (*25*, *26*). The present FRET study utilized the same dye pair, linker arms, and end bases as these previous studies. In addition, all analyses were conducted assuming a value of $^2/_3$ for κ^2, a term describing the relative orientations of the donor and acceptor dipoles for which it is notoriously difficult to determine a value. Of interest was whether the same conditions and assumption would also lead to agreement between FRET and phasing data in determining DNA bend angles. Two such independent techniques can, in the most favorable case, be used together to refine the uncertainties of each technique.

Both the electrophoretic phasing and FRET results support a model of bZIP peptide-induced DNA bending. The phasing results are consistent with those obtained previously: cationic amino acid substitutions resulted in an apparent DNA bend toward the protein-bound face, while anionic substitutions caused apparent DNA bending away from the protein-bound face. The 5′ dye−3′ dye distances determined using FRET were reduced for the charged variant complexes, relative to those in the free duplex and neutral complex. Bending of the DNA helical axis is shown by molecular modeling to be the simplest interpretation of these results. The findings of these two powerful and independent methodologies are thus mutually corroborating and support the hypothesis that the trajectory of DNA can respond to asymmetric changes in local charge density.

EXPERIMENTAL PROCEDURES

Oligonucleotides. Oligonucleotides were synthesized by standard methods on an ABI model 394 instrument. Oligonucleotides were cleaved and deprotected in hot ammonia, purified by denaturing polyacrylamide gel electrophoresis, eluted from the gel, and desalted using C_{18} reverse-phase cartridges (Waters Corp.). Oligonucleotide concentrations were determined at 260 nm, using nearest-neighbor dinucleotide molar extinction coefficients (*28*).

Plasmids. Plasmid pJ013 encodes the basic and leucine zipper regions of GCN4 [amino acids 226−281 (*29*)] subcloned into pET3b (*30*). Plasmids pJT170-2 through pJT170-9 were used as standards in phasing analyses (*31*). Plasmids pDP-AP-1-21, -23, -26, -28, and -30 (*32*) were used to generate probes for phasing analyses. Plasmids pJ170 through pJ175 encode GCN4 variants for expression as crude lysates (*19*). Plasmids pJ290, pJ291, pJ292, pJ299, pJ300, pJ307, and pJ323 encode GCN4 charge variants with N-terminal His_6 fusions.

[1] Abbreviations: DTT, dithiothreitol; EDTA, ethylenediaminetetraacetic acid; FRET, fluorescence resonance energy transfer; HEPES, *N*-(2-hydroxyethyl)piperazine-*N*′-2-ethanesulfonic acid; HPLC, high-performance liquid chromatography; PAGE, polyacrylamide gel electrophoresis; PCR, polymerase chain reaction; TAMRA, tetramethylrhodamine; TBE, Tris−borate−ethylenediaminetetraacetic acid buffer; TBP, TATA box binding protein; TE, Tris-HCl−ethylenediaminetetraacetic acid buffer; Tris, tris(hydroxymethyl)aminomethane.

Construction of His_6-Tagged GCN4 Variants. Standard molecular cloning techniques were employed. PCR was used to append *Bam*HI-compatible termini onto the GCN4 bZIP charge variant coding regions (forward primer, 5′-CTCG-$AGATCTATG_3TCG_3AT$; reverse primer, 5′-GACGAGAT-$CT_3AT_2ACTGTC_2G_2AT_2C$). PCR products were digested with *Bgl*II and inserted into expression plasmid pJ273 that encodes an N-terminal His_6 fusion downstream from an IPTG-inducible promoter. bZIP peptides were expressed in *Escherichia coli* SW1061 cells. Cultures (500 mL) harboring expression plasmids pJ290, pJ291, pJ292, pJ299, pJ300, pJ307, or pJ323 were grown at 37 °C to an OD_{600} of 0.5. IPTG was then added to a final concentration of 0.1 mM, and cells were incubated for an additional 3 h. Cells were pelleted by centrifugation at 5000*g* for 20 min at 4 °C.

Purification of His_6-Tagged GCN4 Variants. All steps were performed at 4 °C. Pelleted cells were resuspended in 10 mL of cold lysis buffer (100 mM NaCl, 20 mM Tris-HCl, pH 8.0, 6 M guanidine) and shaken gently for 5 min. Lysed cell extracts were clarified by centrifugation at 12000*g* for 15 min, and the supernatant was removed to a fresh tube. A spin column (Clontech) was packed with 1.5 mL of Ni-NTA−agarose resin (Qiagen) and charged with 10 mL of cold lysis buffer. Clarified extract was poured over the charged column three times. The column was then washed three times with 6 mL of wash buffer (100 mM NaCl, 20 mM Tris-HCl, pH 8.0, 6 M guanidine, 10 mM imidazole). Protein was eluted from the column with three 1 mL aliquots of elution buffer (100 mM NaCl, 20 mM Tris-HCl, pH 8.0, 6 M guanidine, 100 mM imidazole) and dialyzed exhaustively into a buffer containing 25 mM sodium phosphate, pH 7.5, 1 mM DTT, and 5% glycerol. Protein purity was confirmed via silver staining of 10% Bis-Tris−acrylamide gels (Novex). DNA-binding activity was determined by standard gel-shift methods.

Determination of GCN4 Variant Dissociation Constants. Duplicate experiments were performed at 20 and 4 °C. Peptides were incubated with 50 nM radiolabeled duplex **1** (Figure 1) in 10 μL reactions containing either 10 mM Tris-HCl, pH 7.4, 10 mM KCl, 1 mM EDTA, 2 mM DTT, and 15 ng/μL poly(dI·dC) (20 °C) or 10 mM HEPES, pH 8.0, 20 mM NaCl, 10% glycerol, 1 mM EDTA, 1 mM DTT, 0.05% Triton X-100, and 15 ng/μL poly(dI·dC) (4 °C), with increasing amounts of unlabeled competitor duplex **1** (Figure 1). Solutions were incubated either at 20 °C or on ice for 30 min. Complexes were resolved on native 5% polyacrylamide gels (75:1 acrylamide−bisacrylamide) running in 0.5 × TBE buffer at 10 V/cm. Gels were dried and exposed to storage phosphor screens for analysis using a Molecular Dynamics Storm 840 phosphorimager. K_d values were estimated by measuring the fractional saturation (θ) of the radiolabeled nucleic acid target (T) as a function of the concentration of added protein (P) and fitting to the equation:

$$\theta = \frac{1}{2[\mathrm{T}]_t}\left[[\mathrm{T}]_t + K_d + [\mathrm{P}]_t - \sqrt{([\mathrm{T}]_t + K_d + [\mathrm{P}]_t)^2 - 4[\mathrm{P}]_t[\mathrm{T}]_t}\right] \quad (1)$$

where the subscript t refers to total concentration. The use of eq 1 requires no assumptions with regard to the relative concentrations of T and P and assumes only that the binding reaction is at equilibrium. Measured values of θ were fit to eq 1 with $[P]_t$ and K_d as fitting parameters and $[T]_t$ known. Curve fitting was performed with Kaleidagraph software running on a Macintosh G3 computer.

Electrophoretic Phasing Analyses. Probes for phasing analysis were prepared by PCR from plasmids pDP-AP-1-21, -23, -26, -28, and -30 as previously described (*19*). Pairs of curved DNA standards containing different numbers of phased A_6 tracts at either the center or one terminus of each fragment were prepared by digestion of plasmids pJT170-2 through pJT170-9 with either *Nhe*I and *Bam*HI (*31*). The resulting ~440 bp duplex DNA fragments were purified and radiolabeled as previously described (*19*). Binding studies were performed by incubation of the indicated peptide (~5 nM) with ~100 pM radiolabeled duplex DNA probes (AP-1-21, -23, -26, -28, or -30; see above) in a final reaction mixture of 10 μL containing 10 mM HEPES, pH 8.0, 20 mM NaCl, 10% glycerol, 1 mM EDTA, 1 mM DTT, 0.05% Triton X-100, and 15 ng/μL poly(dI·dC). Solutions were incubated on ice for 30 min. Free and protein-bound DNA probes were resolved by native 8% polyacrylamide gel electrophoresis (29:1 acrylamide−bisacrylamide) in 0.5 × TBE buffer for 20 h at 4 °C (12 V/cm). Dried gels were analyzed by storage phosphor technology. Phasing calculations were performed as previously described (*19*). In these experiments, the factor used to correct for electrophoresis conditions, *k*, was determined to be 1.16 ± 0.01 (*33*).

Determination of End-to-End Distance Distributions for Free and Peptide-Bound DNA Using Time-Resolved Fluorescence Decay. Detailed discussions of the theory of fluorescence resonance energy transfer as well as the methodology and analyses applicable to labeled oligonucleotides have been published (*17*, *25*, *34*−*36*). A summary with details relevant to this study follows. The nonradiative transfer of excited-state energy from a donor fluorophore to an acceptor chromophore through dipole−dipole coupling results in a decrease in the observed fluorescence emission from the donor dye. Since the rate of energy transfer depends on the inverse sixth power of the distance between the donor and acceptor chromophores, changes in that distance are very sensitively reflected in the observed fluorescence decay.

With both fluorophores covalently attached to a DNA oligomer by flexible tethers, the interdye distance is variable rather than fixed. The donor decay then depends on the probability distribution, $P(R)$, of all possible such distances (*37*) in accord with the expression:

$$I_{da}(t) = I_d^0 \int_0^\infty P(R) \sum \alpha_{di} \exp\left[-\left(\frac{t}{\tau_{di}} + \frac{t}{\tau_{D^*}}\left(\frac{R_0}{R}\right)^6\right)\right] dR \quad (2)$$

where the subscripts da and d reference the donor−acceptor labeled oligomer and the donor-only labeled oligomer, respectively. I_d^0 is the initial fluorescence emission intensity from the donor-only labeled oligo, and τ_{di} is the *i*th donor lifetime. Additional relationships include

$$1/\tau_{di} = (k_r + k_f) \quad (3)$$

$$k_t = [(1/\tau_{D^*})(R_0/R)^6] \quad (4)$$

where k_r, k_f, and k_t are the rate constants for nonradiative

decay, fluorescence decay, and energy transfer, respectively, and R_0 is the Förster distance, for which the efficiency of transfer is 0.5. Since only k_l, but not k_t, is dependent on the local environment of the fluorophore, the value of τ_D is uniquely associated with a specific value of R_0 and remains constant as long as the other terms in the R_0 expression remain unchanged. A value of $^2/_3$ for κ^2, the factor describing the relative spatial orientation of the transition dipoles of the dyes, is appropriate for the flexible dye tethers used in this study (*38*; discussed further in the Results section herein). $P(R)$ may thus be extracted from the time-resolved fluorescence decays of the donor-only and donor−acceptor labeled duplexes.

The double-labeled duplex used in this study (duplex **3,** Figure 1) had 5′-TAMRA and 3′-fluorescein attached via 6-carbon linkers to the top strand: TAMRA-5′-GGC**T-GACTCA**TTGG-3′-fluorescein, with the AP-1 sequence in bold. The dyes, linker arms, three 5′-terminal bases, and three 3′-terminal bases are identical to those used previously in similar FRET studies (*17*, *25*−*27*, *34*). Fluorescein and TAMRA constitute a FRET donor−acceptor pair with $R_0 =$ 61 Å, well-suited for determination of the end-to-end distances initially estimated for the AP-1 duplex. The corresponding single-labeled top strand lacked 5′-TAMRA but was otherwise identical (duplex **2**, Figure 1). Both labeled oligonucleotides and the complementary strand were synthesized by Sigma Genosys (The Woodlands, TX). The double- and single-labeled strands were HPLC/PAGE and PAGE purified, respectively. Duplexes were formed with a 2-fold excess of complement. The buffer consisted of 10 mM Tris-HCl, pH 7.4, 10 mM KCl, 1 mM EDTA, 2 mM DTT, and 15 ng/μL poly(dI·dC). All measurements were made at 20 ± 0.05 °C.

Fluorescence decays were obtained for solutions containing 25 nM single-labeled and 50 nM double-labeled duplexes with a total sample volume of 750 μL. The DNA−bZIP complexes were formed by adding 550 nM peptide to ensure >98% DNA saturation according to the equilibrium constants determined from gel-shift assays under identical conditions. These time-resolved emission measurements were made using a LaserStrobe spectrofluorometer (Photon Technology International, Inc., Lawrenceville, NJ) as described previously (*25*).

Data collection and analysis for $P(R)$ were as described previously (*25*). Briefly, detection ranged from just prior to fluorescence emission to ~10 times the longest fluorescence lifetime. For a given sample, three decays were collected and automatically averaged to generate one representative decay curve. The fluorescence decay of the fluorescein donor was extracted from the total emission, which includes the instrument response function, using an iterative reconvolution procedure incorporated into the nonlinear regression analysis. Four such representative curves were generated and defined as one set. These normalized data were fit to both bi- and triexponential decay models, with the relative quality of the fits rigorously assessed according to numerous criteria, including the values of χ^2, the Durbin−Watson parameter (*39*, *40*), and the runs test parameter (*41*). The four α and τ values composing a given set were then averaged; the corresponding average decay curve, termed a composite curve, characterized 12 separate decays. Three such composite curves (a total of 36 curves) were obtained for each of the following conditions: single-labeled AP-1 duplex free and bound to His-PAA, His-EEE, and His-KKK peptides and double-labeled AP-1 duplex free and bound to His-PAA, His-EEE, and His-KKK peptides (Figure 1).

To obtain $P(R)$ for the free duplex, a 3 × 3 matrix was constructed from the three composite decays for the single-labeled duplex and the three composite decays for the corresponding free double-labeled duplex. The resulting nine combinations of donor/donor−acceptor decays were individually analyzed using eq 2 to obtain nine values of $P(R)_{free}$. Nine independent values were thus obtained for $\bar{R}_{free}$ (the mean 5′ dye−3′ dye distance) and for σ_{free} characterizing the width of the distance distribution. These values were averaged to yield the reported values of $\bar{R}_{free}$ and σ_{free} and the corresponding standard deviations. The values of $\bar{R}_{bound}$ and σ_{bound} for the AP-1 duplex bound to His-PAA, His-EEE, and His-KKK were obtained using an identical procedure. Two-tailed *t*-tests were used to evaluate the statistical significance of FRET data using $\bar{R}$ values to four significant figures. Equivalent evaluation of the bend angles utilized the Fisher−Behrens test (for cases of unequal population variances).

To evaluate the effect on dye mobility of bound peptide and of differential peptide charge, time-resolved fluorescein anisotropy measurements were made and analyzed as described (*25*) for the duplex free and bound to all three peptides. The corresponding semi-cone angles were determined as described previously (*25*).

DNA modeling was performed using Insight II (MSI) running on an sgi02 computer.

RESULTS AND DISCUSSION

Protein Expression and Characterization. Figure 1A is based on a published crystal structure of the bZIP domains of GCN4 bound to AP-1 DNA (*16*). Electrostatic interactions (black arrows in Figure 1A) between the DNA sugar−phosphate backbone and the indicated amino acids have been proposed to be responsible for DNA bending by certain charge variants (*19*). Because of the controversy surrounding the interpretation of electrophoretic phasing assays of DNA bending induced by bZIP proteins, we have sought independent approaches to test hypotheses regarding the effect of local charge asymmetry on DNA conformation.

T7-XXX peptides (Figure 1B) refer to GCN4 charge variants characterized previously (*19*). The basic and leucine zipper domains are indicated. The position of the variable amino acid cluster is also highlighted in Figure 1B (**XXX**). PCR and standard subcloning methodologies were used to modify the N-terminus of the T7-XXX peptides and append a hexahistidine tag to create the indicated series of His-XXX peptides (Figure 1B). His-XXX peptides differ from T7-XXX peptides only in the character of their N-termini (highlighted in bold). His-XXX peptides were purified on Ni^{2+}-NTA−agarose columns to greater than 90% homogeneity, as judged by silver staining of SDS−polyacrylamide gels (data not shown). Specific binding of His-XXX peptides to the AP-1 site was demonstrated by gel-shift reactions utilizing nonspecific competitor DNA duplexes (data not shown). Figure 1C displays the DNA duplexes used in these studies. Duplex **1** was used in gel-shift reactions for binding affinity determinations. Duplexes **2** and **3** are single- and double-labeled duplexes used in FRET experiments.

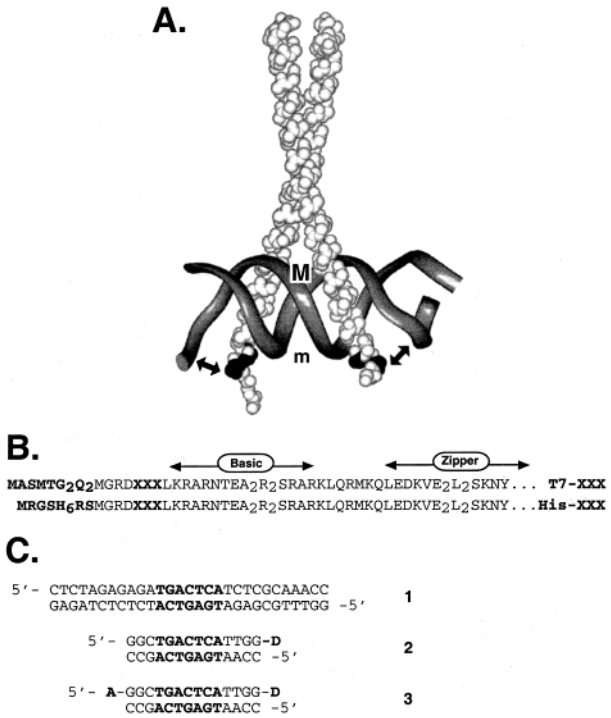

FIGURE 1: bZIP peptides and DNA duplexes under investigation. (A) GCN4 homodimer (peptide backbone atoms shown as white spheres) bound to the AP-1 DNA sequence (ribbon). Locations of amino acid substitutions are indicated by black spheres. Arrows indicate possible electrostatic interactions that might cause DNA bending. DNA major (M) and minor (m) grooves at the center of the AP-1 site are indicated. (B) Amino acid sequences of the recombinant GCN4 derivatives studied. T7-XXX peptides are described in ref *19*. His-XXX peptides differ only in the character of the N-terminus. All peptides also contained the C-terminal sequence HLENEVAELK$_2$LESGQ. Amino acids at positions **XXX** were varied from PAA (wild type, charge = 0) to PAE (−2), PEE (−4), EEE (−6), PAK (+2), PKK (+4), and KKK (+6). Charges refer to the expected charge of the tripeptide region of the dimeric bZIP form. (C) DNA duplexes used in these studies. Duplex **1** (29 bp) was used in gel-shift reactions in binding specificity and dissociation constant determinations. Duplex **2** (14 bp) was singly labeled with 3′-fluorescein which served as the donor species in FRET experiments. Duplex **3** (14 bp) was doubly labeled with both 3′-fluorescein and 5′-TAMRA, which served as a donor/acceptor pair in FRET experiments.

Binding Affinity Determinations. The determination of binding affinities of bZIP charge variants for DNA had not previously been undertaken and was essential to establish conditions required for peptide saturation of target DNA. The equilibrium dissociation constant (K_d) characterizing the affinity of each His-XXX peptide for the AP-1 target DNA sequence was determined by gel-shift reactions. Experiments were performed at both 4 °C (duplex **1**) and 20 °C (duplexes **2** and **3**). Figure 2A displays a representative experiment in which peptide His-PAE (∼200 nM) was incubated with a constant amount (50 nM) of radiolabeled duplex **1**, in the presence of increasing amounts (50 nM to 1.25 μM) of unlabeled competitor duplex **1**. The concentration of His-PAE was empirically determined to shift initially greater than 95% of the labeled duplex **1**. As the concentration of unlabeled duplex **1** is increased, less His-PAE is available to bind labeled duplex **1**, reducing the measured fractional saturation, θ, of labeled duplex **1**. A plot of θ vs the total duplex **1** concentration is shown in Figure 2B. Data were analyzed according to eq 1 in Experimental Procedures.

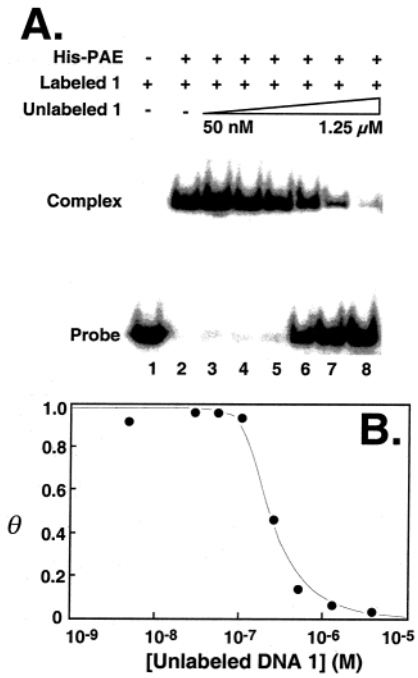

FIGURE 2: Determination of His-XXX peptide binding affinities for AP-1 DNA. (A) Example of a gel-shift experiment with His-PAE binding to radiolabeled DNA duplex **1** in the presence of increasing concentrations of unlabeled duplex **1**. His-XXX peptides were incubated with 50 nM radiolabeled duplex **1**, as described in Experimental Procedures. Reactions also contained the indicated amount of unlabeled competitor duplex **1**. Complexes were resolved from free duplex **1** by electrophoresis on native polyacrylamide gels. (B) Estimation of binding affinity and active protein concentration for His-PAE. θ (fraction of radiolabeled duplex **1** shifted due to peptide binding) is plotted vs the total concentration of labeled and unlabeled duplex **1**. K_d values were estimated through curve fitting to eq 1, as described in Experimental Procedures.

Table 1: Binding Affinities of His-XXX Peptides for Duplex **1**

bZIP peptide	K_d[a] (nM)	bZIP peptide	K_d[a] (nM)
His-PAA	17 ± 5	His-PAK	10 ± 4
His-PAE	12 ± 6	His-PKK	10 ± 3
His-PEE	5 ± 2	His-KKK	6 ± 1
His-EEE	7 ± 1		

[a] K_d values were estimated through curve fitting to eq 1, as described in Experimental Procedures. Mean and standard deviations were obtained from at least four independent measurements.

Curve fitting yields estimates of both K_d and the active peptide concentration in the gel-shift reaction. K_d estimates are displayed in Table 1. Results obtained from experiments performed at either 4 °C (duplex **1**) or 20 °C (duplexes **2** and **3**), under several buffer conditions, were not significantly different. Estimated dissociation constants were between 5 and 15 nM, similar to those reported for other bZIP proteins (*42*, *43*) and for full-length GCN4 (*44*). Analysis of variance indicated that dissociation constants were not significantly different from one another. This result was somewhat unexpected as we had anticipated that cationic charge variants might bind more tightly to AP-1 DNA relative to anionic charge variants, on the basis of attractive electrostatic forces.

Electrophoretic Phasing Assays. Having established binding affinities for purified His-XXX peptides, electrophoretic phasing analyses were employed to measure changes in gel mobility due to the binding of His-XXX peptides. Phasing probes (∼440 bp) contained an array of A_{5-6} tracts located

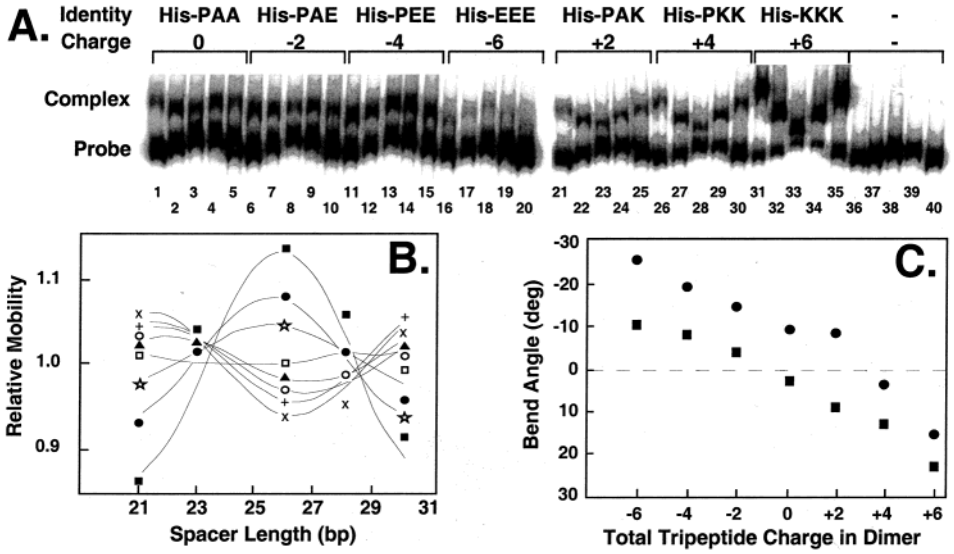

FIGURE 3: Electrophoretic phasing analysis of DNA bending by bZIP charge variants. (A) Electrophoretic mobility shift assay of His-XXX peptides bound to phasing analysis probes. Each set of five lanes contains phasing probes from plasmids pDP-AP-1-21, -23, -26, -28, and -30, respectively, incubated with the homodimer GCN4 charge variants His-PAA (lanes 1−5), His-PAE (lanes 6−10), His-PEE (lanes 11−15), His-EEE (lanes 16−20), His-PAK (lanes 21−25), His-PKK (lanes 26−30), and His-KKK (lanes 31−35). Lanes 36−40 contained no protein. (B) Analysis of phasing data. The relative mobility of each of the five phasing probes in a given protein complex is plotted as a function of the spacing (bp) between the center of the AP-1 site and the center of the A_{5-6} tract array, as described (*19*). Mobilities of free probes (□) and complexes involving His-PAA (▲), His-PAE (○), His-PEE (+), His-EEE (×), His-PAK (☆), His-PKK (●), and His-KKK (■) are shown. (C) Graphical representation of the relation between apparent DNA bend angle and tripeptide formal charge for T7-XXX peptides (●) and His-XXX peptides (■). Positive bend angles are toward the minor groove at the center of the AP-1 site. Error bars are smaller than the symbols used. The axial direction of DNA bending is toward the minor groove (cationic XXX) or major groove (anionic XXX) in a reference frame ~0.5 bp 3′ from the center of the AP-1 site (Figure 1).

at different distances from the AP-1 sequence (*19*). If peptide binding causes DNA bending, as the helical phasing between the two elements (reference A_{5-6} tracts vs His-XXX peptide bound to AP-1 site) changes, electrophoretic mobility is altered. When curvature loci are aligned in cis, gel mobility is minimized. The extent to which gel mobility is reduced in each probe is interpreted as a measure of the DNA bend angle and direction effected by His-XXX peptide binding.

Representative phasing data are presented in Figure 3A. Lanes 36−40 demonstrate the sensitivity of the assay to DNA shape. The AP-1 site possesses a small degree of intrinsic curvature [~6° (*45*)]. Different phasings between the reference A_{5-6} tracts and the unoccupied AP-1 site result in subtle mobility differences of the unbound probes (Figure 3A, lanes 36−40). Mobility retardation is maximal for probe pDP-AP-1-26 (Figure 3A, lane 38), where the loci of curvature are most nearly in phase, suggesting the modest intrinsic curvature of the AP-1 site is toward the minor groove near its center (Figure 1A). Mobility retardation is minimized in probes pDP-AP-1-21 and -30 (Figure 3A, lanes 36 and 40), where the loci of curvature are out of phase.

Changes in electrophoretic mobility induced by His-XXX peptides were then measured. Lanes 1−5 display the mobilities of complexes involving the binding of His-PAA to the phasing probes (Figure 3A, lanes 1−5). Subtle mobility differences are observed among complexes, consistent with a small degree of bending. Mobility anomaly differences are amplified as the charge of the amino acid cluster in the His-XXX peptide dimer is decreased from 0 to −6. Whereas His-PAA (Figure 3A, lanes 1−5) and His-PAE (Figure 3A, lanes 6−10) complexes displayed minor differences in electrophoretic anomaly, mobility differences of DNA probes bound by His-PEE (Figure 3A, lanes 11−15) and His-EEE (Figure 3A, lanes 16−20) were more pronounced. In each complex involving anionic His-XXX peptides, the probe pDP-AP-1-26 was most retarded in the gel, suggesting that the direction of DNA bending is similar in these complexes. A similar result had been observed in our previous studies with T7-XXX peptides and was interpreted as evidence for bending of the AP-1 site away from the anionic amino acid cluster (*19*).

A very different profile of AP-1 probe mobilities was seen in complexes with cationic His-XXX peptides. Whereas sets of DNA probes yielded a pronounced "frown" in the gel when bound by His-PEE and His-EEE, binding of His-PAK (Figure 3A, lanes 21−25), His-PKK (Figure 3A, lanes 26−30), and His-KKK (Figure 3A, lanes 31−35) caused an increasingly pronounced "smile" in the gel. In these cases, mobility retardation was maximal in probe pDP-AP-1-30, suggesting that cationic His-XXX peptides bend the AP-1 site in a direction nearly opposite to that caused by the anionic series.

The gel mobility measurements of each complex were transformed as described previously (*19*). Relative mobility was plotted against the distance in base pairs between the center of the AP-1 site and the center of curvature in the phased A_{5-6} tracts. The results are depicted in Figure 3B. Using techniques derived by Kerppola and co-workers (*33*), the relative differences in probe mobilities were transformed into estimates of DNA bend magnitude and direction due to peptide binding. Estimated DNA bend angles were then plotted against the total charge of the variable amino acid cluster in the peptide dimer (Figure 3C).

The results indicate a similar apparent linear relationship between the DNA bend angle and the total charge of the variable amino acid cluster for both T7-XXX and His-XXX

peptides. In both cases, DNA bending due to peptide binding is maximal for complexes involving either highly anionic (EEE) or cationic (KKK) peptides. However, a global shift of ~10° of bending toward the major groove was observed in the His-XXX peptides, relative to T7-XXX peptides. The distinct vertical displacements of curves in Figure 3C may reflect the overall charge context of the different peptide series (*46*). Overall, the dramatic dependence of the electrophoretic mobilities of these peptide−DNA complexes upon the electrostatic character of six amino acids in T7-XXX and His-XXX peptide dimers confirms our previous data and is most easily interpreted as evidence for DNA bending due to asymmetric changes in the charge density near the DNA sugar−phosphate backbone.

FRET Measurements for Free and bZIP Peptide-Bound AP-1 DNA. The 5′ dye−3′ dye distances for duplex **3** bound to peptides His-PAA, His-EEE, and His-KKK were determined using time-resolved fluorescence emission decay in conjunction with FRET. FRET is the process by which excited-state energy is transferred nonradiatively from a donor to an acceptor chromophore via dipole−dipole coupling. A concomitant decrease in the donor fluorescence emission decay is observed. Since the rate of energy transfer depends exquisitely upon the distance between the donor and acceptor chromophores, the donor decay very sensitively reflects changes in that distance. Time-resolved measurements of the donor emission in FRET reflect only transfer and not static quenching, do not assume a single lifetime, explicitly reflect a distribution of interdye distances, and yield very precise relative mean distances, $\bar{R}$ (*17*, *25*−*27*, *38*). The subtle conformational differences induced in the AP-1 DNA by His-XXX peptides were therefore determined using FRET fluorometry. These spectroscopic results were then considered together with results from electrophoretic phasing assays that have been interpreted as evidence of DNA bending (this work and ref *19*).

To establish the dye mobility and its dependence on peptide binding and peptide charge, time-resolved anisotropy decays were first measured for the donor fluorescein for the labeled AP-1 duplex, free and peptide bound. The full apical angle of the cone describing the rotational motion of the fluorescein linked to the free duplex was calculated to be ~120° and was the same within error for the PAA-, EEE- and KKK-bound duplexes. This cone angle is very similar to those measured previously for both 3′- fluorescein and 5′-TAMRA for a 14mer free and bound to TBP under a variety of conditions (*17*, *25*). This similarity is not surprising since the donor and acceptor dyes, linker arms, three 5′ base pairs, and three 3′ base pairs were identical among these studies. Similar rotational motion was therefore assumed for the AP-1-linked TAMRA. This high level of rotational freedom would be expected to yield a broad range of relative orientations of the dyes' transition moments. The extent of the latter determines the value of the effective κ^2 value.

Because changes in the value of κ^2 yield changed values of R_0 and thus $\bar{R}$, the appropriate value for this term merits further consideration. In principle, one should integrate in eq 2 over a κ^2 distribution, as well as the distance distribution. In the absence of rotation of the donor and acceptor dyes, the a priori width of the κ^2 distribution extends from 0 to 4. However, with dye rotation occurring on a time scale $\geq 10\times$ faster than the average rate of energy transfer and with cone angles of ~120°, the κ^2 distribution extends only from 0.417 to 1.448 (*38*), greatly reducing the uncertainty in the mean κ^2 value relevant to the four AP-1 cases.

Table 2: Lifetime Distributions Characterizing the Donor Fluorescein Emission Decays for Duplexes **2** and **3** Unbound and Bound to Each of the Three GCN4 Peptides

complex	α_1[a]	τ_1 (ns)	α_2	τ_2 (ns)
2	0.414	1.699	0.586	3.540
3	0.760	1.013	0.240	2.133
2 + 2-PAA	0.379	1.657	0.621	3.673
3 + 2-PAA	0.749	1.003	0.251	2.155
2 + 2-KKK	0.474	1.676	0.526	3.554
3 + 2-KKK	0.794	0.976	0.206	2.118
2 + 2-EEE	0.291	1.828	0.709	3.729
3 + 2-EEE	0.696	0.953	0.304	2.161

[a] All donor decay curves, from which probability distributions were determined, were very well fit to a biexponential decay model with the mean value of χ^2 for all 192 curves = 0.959 ± 0.009.

Whereas the κ^2 distribution limits can be determined, the distribution shape is unknown. There is no evidence suggesting variation in the shapes of the AP-1 dye distributions. Furthermore, it has been shown elsewhere that integration over various limited distribution functions, all having the same average value of κ^2 ($^2/_3$), yields $\bar{R}$ values differing only by ≤0.1 Å (*38*). The inverse sixth power dependence of $\bar{R}$ on κ^2 ensures this insensitivity of the value of $\bar{R}$ to small changes in κ^2. The question is therefore: what average κ^2 value should be used? In the previously cited studies of TBP-induced DNA bending (*25*, *26*), which employed FRET probes nearly identical to those used herein, a value of $^2/_3$ was used for κ^2. Because those analyses yielded $\bar{R}$-derived bend angles for the two consensus promoters that were in excellent accord with those determined crystallographically, the same value of κ^2 was used in the present study. These facts, taken together, strongly support the assumption that κ^2 is effectively constant among the four AP-1 conditions with a mean value of $^2/_3$ and that the *relative* values of $\bar{R}$ and corresponding bend angles are highly reliable.

Lifetime distributions were determined for duplexes **2** and **3** (Figure 1C) for the duplexes unbound and bound to the His-PAA, His-KKK, and His-EEE peptides (Table 2). The corresponding mean 5′ dye−3′ dye distances, $\bar{R}$, for duplex **3** were then determined (Table 3). $\bar{R}$ for unbound duplex **3** was 56.6 ± 0.1 Å. Binding of wild-type His-PAA effected a statistically significant 0.2 Å decrease in this distance ($p \leq 0.01$). Binding of both charged mutants, His-KKK and His-EEE, resulted in respective decreases in $\bar{R}$ of 0.6 and 1.0 Å, respectively. These differences in $\bar{R}$ relative to that obtained for DNA·His-PAA are statistically significantly ($p \leq 0.01$). Values of $\bar{R}$ for DNA·His-KKK and DNA·His-EEE are also statistically different from each other ($p \leq 0.01$). These statistical differences remain valid for errors up to 0.3 Å for all cases excepting DNA·His-PAA vs free AP-1 DNA.

Precision in $\bar{R}$ values to 0.1 Å has been demonstrated definitively in a series of recent publications, in which changes in $\bar{R}$ induced by the TATA-binding protein in 14mer duplexes bearing "TATA" sequences were determined using time-resolved FRET (*17*, *25*−*27*). Such precision derives from several sources. A narrow, sharp instrument response function, high signal to noise, and averaging of replicate runs yield raw data curves that are highly reproducible. The

Table 3: Mean 5′ Dye−3′ Dye Distances ($\bar{R}$), Distribution Widths (σ), and Model-Dependent DNA Bend Angles Characterizing Duplex **3** When Free or Bound to bZIP Charge Variants

complex	$\bar{R}^a$ (Å)	σ (Å)	DNA bend angle[b,c] (deg)
3	56.6 ± 0.1	4.6± 0.2	
3 + His-PAA	56.4 ± 0.1	4.7 ± 0.2	9.4 ± 4.0
3 + His-KKK	56.0 ± 0.1	4.5 ± 0.2	16.8 ± 2.2
3 + His-EEE	55.6 ± 0.1	5.6 ± 0.2	21.0 ± 1.8

[a] All $P(R)$s were modeled as constrained shifted Gaussian distributions and corrected for the small amount (<2%) of free duplex as described (*25*). $\bar{R}$ errors ranged from 0.03 to 0.08 Å and were rounded up to 0.1 Å. [b] Bend angles correspond to α, as described in Figure 5. Bend angle error estimates were obtained from standard error propagation theory using the errors in the values of $\bar{R}_{free}$ and $\bar{R}_{bound}$. [c] Bending model with a single central bend, used for describing the bZIP peptide-induced bend in the AP-1 bearing duplex. The bend angles reported are those described by α:

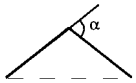

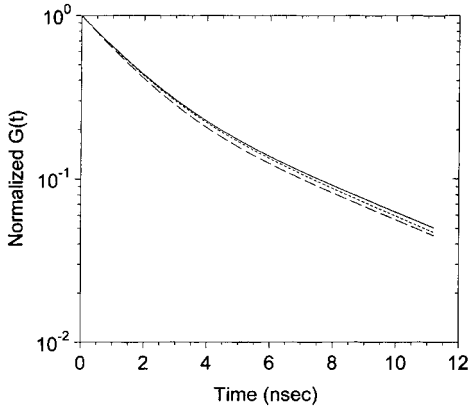

FIGURE 4: $G(t) = F_{DA}(t)/F_D(t)$ is shown for the AP-1 duplex free (smooth line) and bound to His-PAA (short dashes) and His-KKK (long dashes). $G(t)$ represents the hypothetical decay due only to FRET; the area under the curve is the average lifetime for the hypothetical case where only transfer depopulates the donor excited state. For distance distributions having the same width, such as these three, such a plot affords a direct, graphic comparison of $\bar{R}$ values from largest (free AP-1 duplex) to smallest (DNA·His-KKK).

parameters describing each raw decay curve for a given condition are then determined by an extensive search over a broad range of values. The optimal parameters are identified using ~10 stringent criteria. A total of 36 or 48 replicate curves are routinely collected in separate sets and independently analyzed for each condition, yielding, respectively, three or four "composite" curves as described in Experimental Procedures. Nine or 16 independent determinations of $\bar{R}$ are therefore obtained and averaged to yield mean values and corresponding standard deviations. Such ensemble averaging, used to determine ~60 $\bar{R}$ values over a period of several years, has yielded error estimates ranging from 0.03 to 0.14 Å with a mean of <0.1 Å. These estimates have been rounded to 0.1 Å in reporting (*17*, *25*−*27*). This level of precision is consistent with that from steady-state measurements of emission intensity: a change in $\bar{R}$ of ~0.1 Å (for $\bar{R} \sim R_0$) corresponds to an ~1% change in steady-state intensity, with the latter reliably measured using appropriate filtering and dual beam detection.

The widths of the distance distributions (Table 3) reflect both DNA flexibility and the relative dye mobilities. Because the anisotropy decays demonstrate indistinguishable dye mobility for all four cases, differences among the values of σ reported herein must reflect primarily differences in DNA flexibility. These σ values were also highly reproducible, revealing an unexpected but intriguing trend. For DNA free and bound to His-PAA and His-KKK, the values of σ range from 4.5 to 4.7 Å and are statistically indistinguishable. These values are in the very low range of greater than 15 such values measured for free duplexes (*17*, *25*−*27*; unpublished data), suggesting a low level of DNA flexibility for the duplex unbound and PAA and KKK bound. Notably, the value of σ increased ~20% upon binding of DNA to His-EEE ($p \leq 0.001$). To determine the veracity of the latter, the data were analyzed globally with the value of σ constrained to be identical for all three bound cases. This procedure yielded only slightly different bend angle values, ordered as in the unconstrained fitting. However, it significantly decreased the quality of the fit overall and particularly for DNA·His-EEE, suggesting that the larger σ value in the latter reflects a real increase in DNA flexibility in that complex. One interpretation is that electrostatic repulsion between the DNA backbone and the anionic amino acid cluster of His-EEE induces this increased duplex flexibility, which may not be distinguishable from multiple conformers. In contrast, the slight decrease in σ upon DNA binding to His-KKK suggests DNA stiffening due to electrostatic attraction between the DNA backbone and the cationic amino acid cluster.

The donor−acceptor lifetime decay, $F_{DA}(t)$, reflects both the inherent donor decay, $F_D(t)$, and a distribution of lifetimes corresponding to the transfer process. A function that reflects only the pure transfer process, $G(t)$, has thus been generated, with $G(t) = F_{DA}(t)/F_D(t)$. Because $G(t)$ is determined only by $\bar{R}$ and σ, a simple comparison of $\bar{R}$'s is available for distributions having the same σ values. A plot of $G(t)$ for DNA_{free}, DNA·His-PAA, and DNA·His-KKK, all with indistinguishable σ values, therefore reveals directly the ordering of $\bar{R}$ values for these three cases (Figure 4). Additionally, an ~1% decrease in the area of $\int_0^\infty G(t)\,dt$ corresponds to an ~0.1 Å decrease in $\bar{R}$. The decrease in this area between DNA_{free} and DNA·His-PAA, 1.5%, predicts an ~0.15 Å decrease in $\bar{R}$; the calculated decrease is 0.2 Å (Table 3; the remaining difference in area is fully accounted for by the 0.1 Å difference in σ). Similarly, the difference in area between DNA·His-PAA and DNA·His-KKK predicts a further 0.5 Å decrease in $\bar{R}$, compared to the calculated decrease of 0.4 Å (Table 3). Such a direct comparison using the area under the $G(t)$ curve is precluded for DNA·His-EEE because the large difference in σ (~1 Å) for this complex relative to the other cases increases the area by ~5%.

Determination of DNA Bend Angles. Protein-induced DNA deformation can be described by a model-dependent bend angle using the ratio $\bar{R}_{bound}/\bar{R}_{free}$. Such angles successfully characterize and distinguish even subtle conformational changes. The reliability of these bend angles is most convincingly seen within the context of a predictable trend. For example, in the previously mentioned TBP·TATA study,

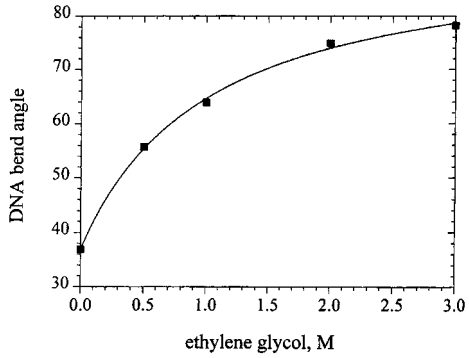

FIGURE 5: Graphical representation of the precision with which model-dependent bend angles may be determined from small changes in $\bar{R}$. These data are from a previous FRET study (*17*) of protein-bound 14mer duplexes that are very similar to those used herein (see Experimental Procedures) and show the dependence of the DNA bend angle on osmolyte concentration. Even such small differences in $\bar{R}$ values yield bend angles (squares) that follow a remarkably smooth trend, as shown in this a posteriori fit of the data to a rectangular hyperbola (line).

the value of $\bar{R}$ determined at five osmolyte concentrations changed incrementally by only 0.1−1.5 Å (Table 3 in ref *17*). The corresponding increases in bend angle range from 3.3° to 18.8° (Table 3 in ref *17*). Despite such small differences, the reliability of these $\bar{R}$ values and derived angles is apparent in the extremely smooth progression of the DNA conformational change from 36.9° to 78.2°, for which all calculated and fitted bend angles are within 0.5° (Figure 5). (For an analogous example, see Table 1 in ref *27*.)

Electrophoretic phasing assays cannot rigorously identify an exact DNA bending locus. However, crystallographic results have shown the DNA deformation in bZIP−DNA complexes to be a single bend centered on the consensus sequence (*11*, *47*). Therefore, we interpret our phasing data in terms of a model in which DNA deformation compresses either the major or minor groove at the center of the AP-1 site. The bend angle, α, may be obtained for the corresponding bending model (Table 3) using the relationship:

$$\bar{R}_{\text{bound}}/\bar{R}_{\text{free}} = \cos\frac{\alpha}{2} \qquad (5)$$

The bend angles corresponding to this model for duplex **3** bound to His-PAA, His-EEE, and His-KKK are shown in Table 3. All three of these bend angles differ significantly ($p < 0.01$). Notably, the magnitudes of these bends are very similar to those determined from phasing analysis. Unlike the latter, FRET measurements give no information regarding the direction of bending. The His-EEE-bound AP-1 duplex undergoes the largest conformational change, with the largest bend and a significant increase in flexibility.

The observed decrease in end-to-end distances for DNA duplex **3** bound by anionic or cationic forms of His-XXX peptides relative to the neutral form is consistent with DNA bending near the center of the AP-1 site. Because of the helical nature of DNA, we also considered the possibility that similar changes in end-to-end distance could arise from other changes in DNA geometry, rather than bending of the helix axis. Significant DNA twisting or untwisting has not been reported in crystal structures of bZIP proteins nor have changes in base pair spacing been observed. It remains theoretically possible, however, that changes in dye−dye distances reflect changes in the helical alignment of the fluorophores due to peptide-induced changes in DNA rise or twist, apart from axial bending.

Molecular models of DNA duplex **3** were therefore constructed to explore the effect on predicted dye−dye distances of changing the helical rise and twist parameters of the DNA (between the base pairs of the 7 bp AP-1 site). We began by using straight models of duplex **3** with rise and twist parameters of 3.2 Å and 34°, as observed in the GCN4/DNA X-ray structure (*16*) where no deviations from B-form DNA were observed in the complex with wild-type GCN4. When no DNA axial bending was allowed, we noted that decreases in average dye−dye distances on the order of the observed 0.6 Å would require either a decreased rise per base pair of ∼0.1 Å over the AP-1 site (with no change in twisting), an untwisting of ∼4° per base pair over the same AP-1 site (with no change in base pair rise), or some combination of these two distortions. Such distortions in DNA geometry in bZIP−DNA complexes have not been observed by X-ray techniques (*11*, *47*, *48*). DNA untwisting by ∼4° per base pair would convert the helical repeat of the AP-1 site from 10.6 bp per turn to 12.0 bp per turn. It is important to note that these changes would be required in the geometries of DNA bound to both His-EEE and His-KKK peptides relative to the DNA geometry when bound by His-PAA. The similar decreases in $\bar{R}$ for oppositely charged peptide variants would seem more consistent with DNA bending rather than unprecedented changes in DNA base pair rise and twist. If such unprecedented changes were induced, one might expect cationic and anionic bZIP variants to have different effects on the organization of base pairs within the AP-1 site, inconsistent with our FRET measurements. The fact that apparent DNA bend direction in all cases remains centered within 0.5 bp from the center of the AP-1 site also argues against twist distortions of the DNA.

We favor an interpretation wherein reductions in $\bar{R}$ upon binding of duplex **3** to the His-XXX peptides reflect bending of the DNA helix axis due to asymmetric changes in the charge density near the DNA backbone. Together with previous results (*19*), the present electrophoretic phasing results and the highly precise FRET measurements provide independent and mutually supportive evidence of electrostatically induced DNA bending.

Conclusion. Purified GCN4 bZIP peptide derivatives having differential charge mutations near the DNA backbone are shown to yield phase-dependent alterations in gel mobility. In addition, opposite charges are shown to result in opposite directions of apparent DNA bending, consistent with previous observations (*19*). All of these bZIP domains have similar DNA affinities. That anomalous gel mobility does *not* derive from differences in bZIP structural details has been reported elsewhere from studies employing bZIP fusion proteins (*46*). These results support strongly the electrostatic model for DNA bending described herein.

These same GCN4 peptides are shown by FRET to induce a decreased end-to-end distance in AP-1 bearing duplexes, consistent with DNA bending. The bends induced by the cationic or anionic variants are 79% and 123% larger, respectively, than those from the neutral peptide. The magnitudes of these charge variant-induced bends are in very good accord with those determined from phasing analysis.

Similar reductions in dye−dye distances without axial bending could be achieved only by significant changes in DNA twist and/or rise parameters within the AP-1 site for bZIP peptide charge variants. Such DNA distortions have not been observed in crystal structures of bZIP−DNA complexes, even in the case of Jun and Fos, where a similar pattern of cationic amino acids occurs naturally. Taken together, these complementary results thus support a model in which DNA bending can be induced by the binding of appropriately charged peptides at low ionic strength.

ACKNOWLEDGMENT

We thank M. Doerge in the Mayo Foundation Molecular Biology Core Facility for providing excellent oligonucleotide synthesis services. We also thank Z. Bajzer in the Mayo Biomathematics Resource for curve fitting advice and A. Schepartz for the gift of phasing plasmids.

REFERENCES

1. Kahn, J. D., and Crothers, D. M. (1993) in *Cold Spring Harbor Symposia on Quantitative Biology*, pp 115−122, Cold Spring Harbor Laboratory Press, Cold Spring Harbor, NY.
2. Luger, K., Mader, A. W., Richmond, R. K., Sargent, D. F., and Richmond, T. J. (1997) Crystal structure of the nucleosome core particle at 2.8 Å resolution, *Nature 389*, 251−260.
3. Parkinson, G., Wilson, C., Gunasekera, A., Ebright, Y. W., Ebright, R. E., and Berman, H. M. (1996) Structure of the CAP-DNA complex at 2.5 Å resolution: A complete picture of the protein-DNA interface, *J. Mol. Biol. 260*, 395−408.
4. Maher, L. J. (1998) Mechanisms of DNA bending, *Curr. Opin. Chem. Biol. 2*, 688−694.
5. Kim, Y., Greiger, J. H., Hahn, S., and Sigler, P. B. (1993) Crystal structure of a yeast TBP/TATA-box complex, *Nature 365*, 512−520.
6. Pontiggia, A., Rimini, R., Harley, V. R., Goodfellow, P. N., Lovell-Badge, R., and Bianchi, M. E. (1994) Sex-reversing mutations affect the architecture of SRY-DNA complexes, *EMBO J. 13*, 6115−6124.
7. Schultz, S. C., Shields, G. C., and Steitz, T. A. (1991) Crystal structure of a CAP-DNA complex: The DNA is bent by 90°, *Science 253*, 1001−1007.
8. Williams, L. D., and Maher, L. J. (2000) Electrostatic mechanisms of DNA deformation, *Annu. Rev. Biophys. Biomol. Struct. 29*, 497−521.
9. Mirzabekov, A. D., and Rich, A. (1979) Asymmetric lateral distribution of unshielded phosphate groups in nucleosomal DNA and its role in DNA bending, *Proc. Natl. Acad. Sci. U.S.A. 76*, 1118−1121.
10. Manning, G. S., Ebralidse, K. K., Mirzabekov, A. D., and Rich, A. (1989) An estimate of the extent of folding of nucleosomal DNA by laterally asymmetric neutralization of phosphate groups, *J. Biomol. Struct. Dyn. 6*, 877−889.
11. Glover, J. N., and Harrison, S. C. (1995) Crystal structure of the heterodimeric bZIP transcription factor c-fos-c-jun bound to DNA, *Nature 373*, 257−261.
12. Kerppola, T. K., and Curran, T. (1991) Fos-Jun heterodimers and Jun homodimers bend DNA in opposite orientations: implications for transcription factor cooperativity, *Cell 66*, 317−326.
13. Kerppola, T. K., and Curran, T. (1993) Selective DNA bending by a variety of bZIP proteins, *Mol. Cell. Biol. 13*, 5479−5489.
14. Paolella, D. N., Liu, Y., and Schepartz, A. (1997) Electrostatic mechanism for DNA bending by bZIP proteins, *Biochemistry 36*, 10033−10038.
15. Leonard, D. A., Rajaram, N., and Kerppola, T. K. (1997) Structural basis of DNA bending and oriented heterodimer binding by the basic leucine zipper domains of Fos and Jun, *Proc. Natl. Acad. Sci. U.S.A. 94*, 4913−4918.
16. Ellenberger, T. E., Brandl, C. J., Struhl, K., and Harrison, S. C. (1992) The GCN4 basic region leucine zipper binds DNA as a dimer of uninterrupted α helices: Crystal structure of the protein-DNA complex, *Cell 71*, 1223−1237.
17. Wu, J., Parkhurst, K. M., Powell, R. M., and Parkhurst, L. J. (2001) DNA sequence-dependent differences in TATA-binding protein-induced DNA bending in solution are highly sensitive to osmolytes, *J. Biol. Chem. 276*, 14623−14627.
18. Strauss-Soukup, J. K., and Maher, L. J. (1997) DNA bending by GCN4 mutants bearing cationic residues, *Biochemistry 36*, 10026−10032.
19. Strauss-Soukup, J., and Maher, L. J. (1998) Electrostatic effects in DNA bending by GCN4 mutants, *Biochemistry 37*, 1060−1066.
20. Sitlani, A., and Crothers, D. (1998) DNA-binding domains of Fos and Jun do not induce DNA curvature: an investigation with solution and gel methods, *Proc. Natl. Acad. Sci. U.S.A. 95*, 1404−1409.
21. Sitlani, A., and Crothers, D. M. (1996) Fos and jun do not bend the AP-1 recognition site, *Proc. Natl. Acad. Sci. U.S.A. 93*, 3248−3252.
22. Kerppola, T. K. (1996) Fos and Jun bend the AP-1 site: Effects of probe geometry on the detection of protein-induced DNA bending, *Proc. Natl. Acad. Sci. U.S.A. 93*, 10117−10112.
23. Kerppola, T. K., and Curran, T. (1997) The transcription activation domains of Fos and Jun induce DNA bending through electrostatic interactions, *EMBO J. 16*, 2907−2916.
24. Kerppola, T. K. (1997) Comparison of DNA bending by Fos-Jun and phased A tracts by multifactorial phasing analysis, *Biochemistry 36*, 10872−10884.
25. Wu, J., Parkhurst, K. M., Powell, R. M., Brenowitz, M., and Parkhurst, L. J. (2001) DNA bends in TATA-binding protein-TATA complexes in solution are sequence dependent, *J. Biol. Chem. 276*, 14614−14622.
26. Powell, R. M., Parkhurst, K. M., Brenowitz, M., and Parkhurst, L. J. (2001) Marked stepwise differences within a common kinetic mechanism characterize TATA-binding protein interactions with two consensus promoters, *J. Biol. Chem. 276*, 29782−29791.
27. Powell, R. M., Parkhurst, K. M., and Parkhurst, L. J. (2002) Comparison of TATA-binding protein recognition of a variant and consensus DNA promoters, *J. Biol. Chem. 277*, 7776−7784.
28. Puglisi, J. D., and Tinoco, I. (1989) Absorbance melting curves of RNA, *Methods Enzymol. 180*, 304−325.
29. Suckow, M., von Wilcken-Bergmann, B., and Muller-Hill, B. (1993) Identification of three residues in the basic regions of the bZIP proteins GCN4, C/EBP and TAF-1 that are involved in specific DNA binding, *EMBO J. 12*, 1193−1200.
30. Studier, F. W., Rosenberg, A. H., Dunn, J. J., and Dubendorff, J. W. (1990) Use of T7 RNA polymerase to direct expression of cloned genes, *Methods Enzymol. 185*, 60−89.
31. Thompson, J. F., and Landy, A. (1988) Empirical estimation of protein-induced DNA bending angles: applications to λ site-specific recombination complexes, *Nucleic Acids Res. 16*, 9687−9705.
32. Paolella, D. N., Palmer, C. R., and Schepartz, A. (1994) DNA targets for certain bZIP proteins distinguished by an intrinsic bend, *Science 264*, 1130−1133.
33. Kerppola, T. K. (1994) DNA bending specificity among bZIP family proteins in *Transcription: mechanisms and regulation* (Conaway, R. C., and Conaway, J. W., Eds.) pp 387−424, Raven Press, New York.
34. Parkhurst, K. M., Richards, R. M., Brenowitz, M., and Parkhurst, L. J. (1999) Intermediate species possessing bent DNA are present along the pathway to formation of a final TBP-TATA complex, *J. Mol. Biol. 289*, 1327−1341.
35. Parkhurst, K. M., and Parkhurst, L. J. (1995) Donor−acceptor distance distributions in a double-labeled fluorescent oligonucleotide both as a single strand and in duplexes, *Biochemistry 34*, 293−300.
36. Parkhurst, K. M., and Parkhurst, L. J. (1995) Kinetic studies by fluorescence resonance energy transfer employing a double-label oligonucleotide: hybridization to the oligonucleotide complement and to single-stranded DNA, *Biochemistry 34*, 285−292.
37. Cantor, C. R., and Pechukas, P. (1971) Determination of distance distribution functions by singlet−singlet energy transfer, *Proc. Natl. Acad. Sci. U.S.A. 68*, 2099−2101.
38. Parkhurst, L. J., Parkhurst, K. M., Powell, R. M., Wu, J., and Williams, S. L. (2002) Time-resolved FRET studies of DNA bending in double-stranded oligonucleotides and in DNA-protein complexes, *Nucleic Acids Sci*. (in press).
39. Durbin, J., and Watson, G. S. (1950) Testing for serial correlation in least squares regression. I, *Biometrika 37*, 409−428.
40. Durbin, J., and Watson, G. S. (1951) Testing for serial correlation in least squares regression. II, *Biometrika 38*, 159−178.

41. Hamburg, M. (1974) *Basic Statistics: A modern approach*, Harcourt Brace Jovanovich, New York.
42. Williams, J. S., Dixon, J. E., and Andrisani, O. (1993) Binding constant determination studies utilizing recombinant delta-creb protein, *DNA Cell Biol. 12*, 183−190.
43. Cao, Z., Umek, R. M., and McKnight, S. L. (1991) Regulated expression of three C/EBP isoforms during adipose conversion of 3T3-L1 cells, *Genes. Dev. 5*, 1538−1552.
44. Hope, I. A., and Struhl, K. (1985) GCN4 protein, synthesized in vitro, binds HIS3 regulatory sequences: implications for general control of amino acid biosynthetic genes in yeast, *Cell 43*, 177−188.
45. Tomky, L. A., Strauss-Soukup, J. K., and Maher, L. J. (1998) Effects of phosphate neutralization on the shape of the AP-1 transcription factor binding site in duplex DNA, *Nucleic Acids Res. 26*, 2298−2305.
46. Hardwidge, P. R., Kahn, J. D., and Maher, L. J. (2002) Dominant effect of protein charge rather than protein shape in apparent DNA bending by engineered bZIP domains *Biochemistry* (in press).
47. Chen, L., Glover, J. N., Hogan, P. G., Rao, A., and Harrison, S. C. (1998) Structure of the DNA-binding domains of NFAT, Fos and Jun bound specifically to DNA, *Nature 392*, 42−48.
48. Konig, P., and Richmond, T. J. (1993) The X-ray structure of the GCN4-bZIP bound to ATF/CREB site DNA shows the complex depends on DNA flexibility, *J. Mol. Biol. 233*, 139−154.

BI020213W